



Local phonon mode in thermoelectric $\text{Bi}_2\text{Te}_2\text{Se}$ from charge neutral antisites

Yao Tian,¹ Gavin B. Osterhoudt,² Shuang Jia,^{3,a)} R. J. Cava,³ and Kenneth S. Burch^{2,b)}¹*Department of Physics and Institute of Optical Sciences, University of Toronto, Toronto, Ontario M5S 1A7, Canada*²*Department of Physics, Boston College, 140 Commonwealth Ave., Chestnut Hill, Massachusetts 02467-3804, USA*³*Department of Chemistry, Princeton University, Princeton, New Jersey 08540, USA*

(Received 22 October 2015; accepted 13 January 2016; published online 28 January 2016)

Local modes caused by defects play a significant role in the thermal transport properties of thermoelectrics. Of particular interest are charge-neutral defects that suppress thermal conductivity, without significantly reducing electrical transport. Here, we report a temperature dependent Raman study that identifies such a mode in a standard thermoelectric material, $\text{Bi}_2\text{Te}_2\text{Se}$. One of the modes observed, whose origin has been debated for decades, was shown most likely to be an antisite defect induced local mode. The anomalous temperature independent broadening of the local mode is ascribed to the random arrangement of Se atoms. The temperature renormalization of all modes is well explained by an anharmonic model–Klemens’s model. © 2016 AIP Publishing LLC.

[<http://dx.doi.org/10.1063/1.4941022>]

The family of compounds, $\text{Bi}_2\text{Te}_{3-x}\text{Se}_x$, have been studied for decades as good thermoelectrics.¹ In binary compounds like Bi_2Se_3 and Bi_2Te_3 , the small defect formation energies and band gaps often result in relatively large carrier densities, leading the bulk conductance to dominate over the surface conductance.² A transition from p-type to n-type behavior in the $\text{Bi}_2\text{Te}_{3-x}\text{Se}_x$ solid solution was reported decades ago.^{3,4} Further studies have revealed that when x is close to 1, namely, $\text{Bi}_2\text{Te}_2\text{Se}$, the crystal structure is ordered.² The ordering was suggested to produce the dramatic reduction in defect density.⁵ However, surprisingly it has been known that $\text{Bi}_2\text{Te}_2\text{Se}$ contains a single extra mode, the origin of which remains a mystery and was suspected to be a local mode.⁶ It is known that local modes play an important role in lowering the thermal conductivity of materials. Especially for thermoelectric clathrates⁷ and skutterudites,⁸ intentionally induced local modes (rattling modes) can cause glassy behavior in phonon transport, while producing little, if any effect on the electronic properties, namely, phonon-glass electron-crystal. Raman spectroscopy, owing to its non-destructive nature and quick access to phonon modes, has been widely used for characterization of materials for decades. Moreover, Raman scattering can be used to probe the temperature dependence of the phonon dynamics,^{9–12} as well as defects and defects-induced local modes.^{13–15} Although there have been many studies on $\text{Bi}_2\text{Te}_{3-x}\text{Se}_x$ using Raman spectroscopy,^{6,16} a high spectral resolution broad temperature range dependent study is still lacking.

In this paper, we present a Raman study of $\text{Bi}_2\text{Te}_2\text{Se}$ over the temperature range from 10 K to 290 K. Four modes were observed in the whole temperature range. Three of them are assigned as A_g^1 , E_g , and A_g^2 modes.⁶ The extra mode, the origin of which is controversial, is shown most likely to be an antisite defects-induced local mode. The

anomalous broadness of the local mode is qualitatively understood through a simulation of diatomic chains. The temperature dependence of all four phonon modes is well explained by anharmonic phonon-phonon interactions.

The $\text{Bi}_2\text{Te}_2\text{Se}$ single crystal was grown with special techniques to suppress carrier-concentration. Detailed growth procedure and characterizations are described in previously published works.^{2,17,18} In preparation for measurements, the $\text{Bi}_2\text{Te}_2\text{Se}$ sample was freshly cleaved and quickly placed inside a sample chamber. The temperature dependence was achieved via an automated closed-cycle cryostation manufactured by Montana Instruments, Inc. The Raman spectra were taken in a backscattering configuration with a home-built Raman microscope. A linear polarized 532 nm solid state laser was used as the excitation source. Two diffractive Notch Filters were used to reject Rayleigh scattering. This also allows us to observe both Stokes and anti-Stokes Raman shifts. The laser spot size was 1 μm in diameter. The laser power was kept as low as 40 μW to avoid laser-induced heating. This was checked at 10 K by monitoring the anti-Stokes signal as the laser power was reduced. Once the anti-Stokes signal disappeared, an additional 50% of the power was cut. More details about the instruments can be found elsewhere.^{19–22}

$\text{Bi}_2\text{Te}_2\text{Se}$ is of a quintuple layer structure $\text{Te}_I\text{-Bi-Te}_{II}\text{-Bi-Te}_I$ (see Fig. 1(a)).² From group theory analysis, the space group of $\text{Bi}_2\text{Te}_2\text{Se}$ is $R\bar{3}m$ (No.166). The point group is D_{3d} . There are four inequivalent irreducible representations in the D_{3d} point group. They are A_g , E_g , A_u , and E_u , respectively. Raman-active modes are $2A_g + 2E_g$. As established in previous experiments, the lowest energy mode in the $\text{Bi}_2\text{Te}_{3-x}\text{Se}_x$ is typically below 50 cm^{-1} which is below our low energy cut-off.^{23–25} As a result, in our spectral range, we expect to observe three phonon peaks from the zone center modes in the Raman spectra of $\text{Bi}_2\text{Te}_2\text{Se}$.

The spectra of $\text{Bi}_2\text{Te}_2\text{Se}$ taken at 290 K and 10 K under XX configuration (collinear polarized) are shown in Fig. 1(b). We can see that the $\text{Bi}_2\text{Te}_2\text{Se}$ spectra consist of two isolated peaks at lower frequencies, and two peaks at higher energies

^{a)}Current address: School of Physics, Peking University, Beijing 100871, China.

^{b)}Electronic mail: ks.burch@bc.edu

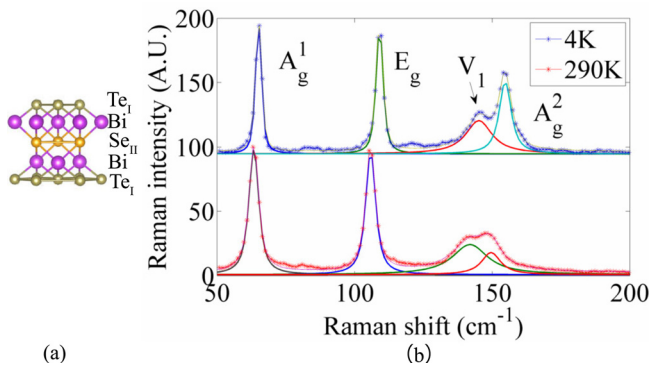


FIG. 1. (a) Schematic crystal structures of $\text{Bi}_2\text{Te}_2\text{Se}$. (b) Raman spectra of $\text{Bi}_2\text{Te}_2\text{Se}$ taken at 4 K and 290 K under XX (colinear polarized) configuration. Raw data are shown by * markers. The four individual Voigt functions are shown in different colors. The added curves are shown by thinner lines.

which overlap. To quantitatively evaluate the overlapped features, the Raman spectra of $\text{Bi}_2\text{Te}_2\text{Se}$ were fitted with four Voigt functions (more details about the Voigt function are given later). From the fit, the frequencies of the four features are: 65.12 cm^{-1} , 109.1 cm^{-1} , 145.0 cm^{-1} , and 154.6 cm^{-1} at 10 K, which are in good agreement with those found by Akrap *et al.*²⁶ However, the line-width in our spectra is much narrower, perhaps due to the higher quality of our crystal. In Fig. 2, we also show the Raman spectra of $\text{Bi}_2\text{Te}_2\text{Se}$ under XY (crossed polarized) configuration at room temperature. It is clear that all the modes except the one located at 109.1 cm^{-1} vanish in XY configuration which is consistent with the literature.⁶ The first two modes plus the mode of highest energy have been assigned as A_g^1 , E_g , and A_g^2 modes according to the literature.⁶ However, there is no consensus on the assignment of the mode at 145.0 cm^{-1} , which we denote as V_1 for convenience. Akrap *et al.* noted that a very weak mode seen in their IR conductivity spectra was very close to the V_1 mode. From this, the authors concluded that the appearance of this mode in Raman scattering is probably due to the activation of the A_{2u} mode by disorder and symmetry breaking. Given the similar energy and temperature induced broadening of phonon linewidth from 10 K to 290 K (3 cm^{-1} broadening for V_1 mode, and 3.6 cm^{-1} for A_g^2 mode), one would expect a similar temperature independent broadening at low temperature. However, as described below, we found that upon cooling to 10 K, the A_g^2 mode becomes much narrower, as it is typically observed, while

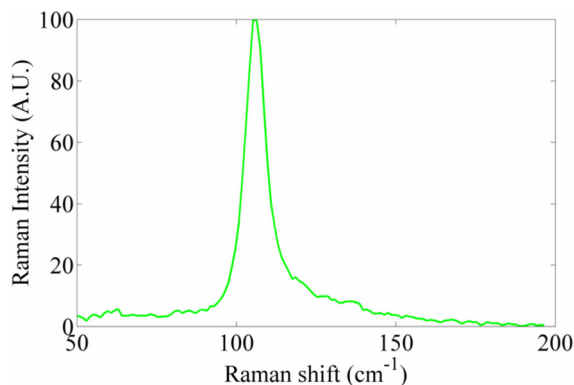


FIG. 2. Raman spectra of $\text{Bi}_2\text{Te}_2\text{Se}$ under XY (crossed polarized) configuration at room temperature.

the V_1 mode remains considerably broad. Perhaps, more problematic, disorder, or symmetry-breaking induced IR modes in Raman spectra are typically very weak²⁷ and cannot be as strong as ordinary Raman modes (especially when one compares the V_1 mode to the A_g^2 mode at room temperature).

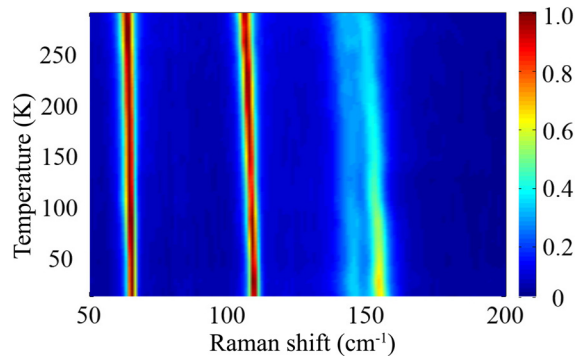
Richter and Becker⁶ also observed this mode and suspected it to be a splitting of the A_g^2 mode resulting from the local change in bonds between the different chalcogenide layers (i.e., Se in the middle of the quintuple versus Te in the outer layers). However, these measurements were performed at room temperature and thus one could not tell whether this was indeed a local mode. Defects could also enable non-zone center phonons to appear in the Raman spectra, as is typically seen in graphite (i.e., the D-band). This mechanism can generate a broad Raman profile due to the participation of multiple modes.²⁸ This phenomenon is usually related to electronic resonance effect. Nonetheless, this possibility also seems unlikely, when comparing $\text{Bi}_2\text{Te}_2\text{Se}$ with Bi_2Te_3 . Specifically, Bi_2Te_3 has a large density of Bi_{Te} antisite defects that generally lead to its heavy p-type doping.^{2,29} Considering the high similarity in both electronic and phonon structures between Bi_2Te_3 and $\text{Bi}_2\text{Te}_2\text{Se}$, one should also observe a “ V_1 -like” mode in Bi_2Te_3 .²⁵ Nonetheless, despite extensive Raman measurements by various groups, the V_1 mode has only been observed in samples with Se doping.^{6,30}

The comparison with Bi_2Te_3 suggests we carefully consider the role of Se in generating this new Raman mode. In theory, Se enters the Se_{II} site and not the Te_{I} site. Nonetheless, scanning tunneling microscopy (STM) studies have established several types of defects.²⁹ They are adatoms remnant from the cleavage process, $\text{Te}_{\text{I}}\text{-Se}_{\text{II}}$ antisites, $\text{Te}_{\text{I}}\text{-Bi}$ antisites, and $\text{Se}_{\text{I}}\text{-Bi}$ antisites, respectively. A further study using x-ray diffraction (XRD) showed in $\text{Bi}_2\text{Te}_2\text{Se}$ 8.5% of Se_{II} atoms are replaced by Te and 4.17% of Te_{I} atoms are substituted by Se. The site occupancy factor of Bi is 1.2. Therefore, the Se-Te antisite is the major defect in $\text{Bi}_2\text{Te}_2\text{Se}$. A point defect, such as the Te-Se antisite, can cause a local mode that vibrates at its own frequency with a considerably broad line-width.¹⁵ Such local modes have been observed in many semiconductors like Ge-Si alloys,³¹ $\text{CdSe}_{0.985}\text{S}_{0.015}$,³² $\text{Ba}_y\text{Sr}_{1-y}\text{F}_2$,³³ $\text{Sr}_y\text{Ca}_{1-y}\text{F}_2$,³³ and so on. A similar temperature dependence of the line-width has been observed in Iodine intercalated $\text{Bi}_2\text{Sr}_2\text{CuO}_6$.³⁴ The I_3^- line narrows (19 cm^{-1} to 16 cm^{-1}) from room temperature to 30 K but remains considerably broad, very similar to our observation (14.4 cm^{-1} to 11.7 cm^{-1}). Besides, the intensity of a defect mode can be strong and comparable to other phonon modes as observed in GaN and Co-doped ZnO films.^{35,36} Thus, it is very likely the V_1 mode is a local mode caused by the point defect Te-Se antisite.

To gain more quantitative insights, we focus on the temperature dependent Raman spectra of $\text{Bi}_2\text{Te}_2\text{Se}$ over the whole temperature range (shown in Fig. 3). We fit the Raman spectra with Voigt profile functions

$$V(x, \sigma, \Omega, \Gamma) = \int_{-\infty}^{+\infty} G(x', \sigma) L(x - x', \Omega, \Gamma) dx', \quad (1)$$

which is the convolution of Gaussian and Lorentzian functions. The Gaussian is employed to account for the instrumental resolution and the Lorentzian represents a phonon

FIG. 3. The temperature dependent Raman spectra of $\text{Bi}_2\text{Te}_2\text{Se}$.

mode. The half width σ of the Gaussian was determined by the instrumental resolution, which is 1.8 cm^{-1} in our system. The extracted temperature dependent phonon shifts Ω and line-widths Γ are shown in Fig. 4.

From the plot, we can see that all phonon modes sharpen and harden as the temperature is decreased. This naturally results from the anharmonic phonon-phonon interaction which leads to a renormalization of phonon shifts and line-widths. To analyze the temperature dependent behavior, Klemens's model was used, which is only an approximation to the phonon-phonon interaction, but widely used to interpret anharmonicity.^{16,37} In this model, an optical phonon is assumed to decay into two phonons with opposite momentum. The "coalescence" process where a phonon and a second phonon fuse into a third phonon is neglected, because it requires an existing population of phonons, which are very small at low temperatures.³⁸ Klemens's model reads³⁹

$$\Omega(\omega, T) = \Omega_0 + C[2n_B(\omega_0/2) + 1], \quad (2)$$

$$\Gamma(\omega, T) = \Gamma_0 + A[2n_B(\omega_0/2) + 1], \quad (3)$$

where Γ_0 can be interpreted as the contribution from the crystalline disorder, Ω_0 is the harmonic phonon shift, n_B is the Bose-Einstein function, and A and C are the coefficients

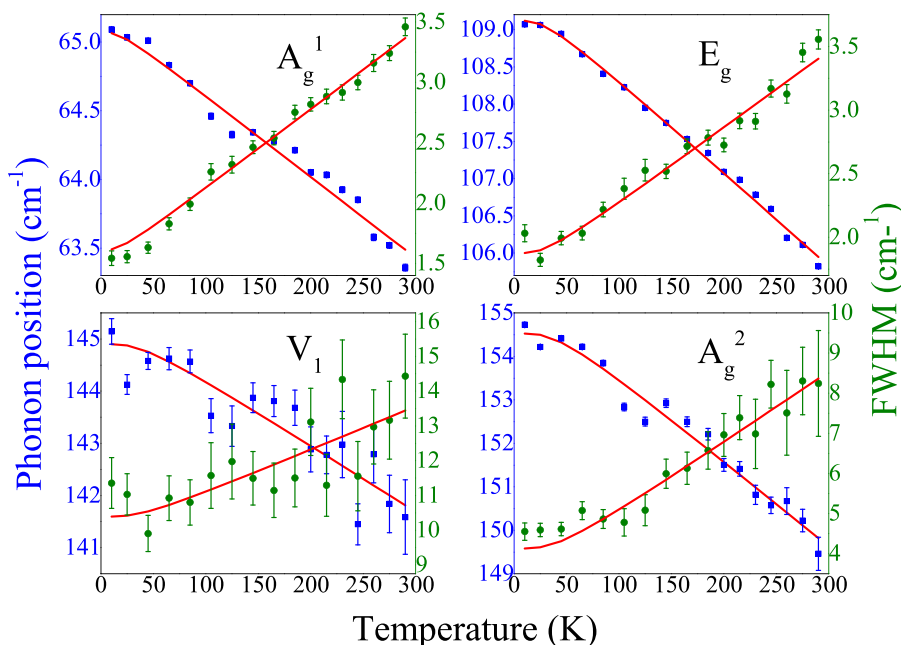
TABLE I. Anharmonic parameters of $\text{Bi}_2\text{Te}_2\text{Se}$. The unit is cm^{-1} .

$\text{Bi}_2\text{Te}_2\text{Se}$								
Mode	ω_0	Error	C	Error	Γ_0	Error	A	Error
A_g^1	65.3	0.1	-0.14	0.01	1.50	0.05	0.15	0.01
E_g	109.6	0.1	-0.50	0.01	1.64	0.08	0.24	0.02
V_1	145.7	0.4	-0.67	0.11	9.73	0.73	0.66	0.19
A_g^2	155.7	0.3	-1.1	0.10	3.14	0.29	1.00	0.08

representing three-phonon (cubic) interactions. The resulting fits are also shown in Fig. 4. Judging for all the figures, we can see that the model works very well. The complete fit parameters including errors are listed in Table I. Among all the modes, the temperature independent Γ_0 is dramatically larger for the V_1 mode, almost three times that of the A_g^2 mode. However, the A and C follow the trend of increasing as a function of phonon frequency.

To qualitatively explain this, we employed statistical analysis which was used to handle disordered effects.⁴⁰ We can think of the $\text{Bi}_2\text{Te}_2\text{Se}$ crystal as constituted of many atomic chains. Raman modes in $\text{Bi}_2\text{Te}_2\text{Se}$ only involve Bi and Te_l sites,⁶ thus, a perfect chain consists of Bi and Te atoms one after the other. Since our sample has defects, some Te atoms will be randomly replaced by Se atoms. The energies of the local modes in these chains have much larger dependence on the configuration of Se atoms in the chain than that of a normal phonon mode. Consequently, the observed spectra consist of many local modes with slightly different frequencies, resulting in much larger broadening than normal phonon modes.

To test the validity of the above statements, a simple model adopted from the literature¹⁵ was used to calculate the vibrational modes of a one dimensional circular diatomic chain. The original chain consists of 48 atoms of two types of atoms (a,b) with the configuration $\dots a - b - a - b \dots$. The mass of atom a (b) was set to be 2.58 (4). The force constant was set to be 1. To simulate the local modes, two atoms a

FIG. 4. Temperature dependence of the shifts and line-widths of phonons of $\text{Bi}_2\text{Te}_2\text{Se}$.

were replaced by a “defect” atom c with mass 1.57. The masses were chosen based on the real mass ratio of Te (a), Bi (b), and Se (c) atoms. The number of the “defect” atom c was chosen to represent 4.17% disorder obtained by XRD. Since two atoms are replaced, there will be two local modes in the chain. Twenty trials were run and for each trial two sites of atom a were randomly chosen to be replaced by atom c . The results of two local modes as well as a non-local mode (phonon mode) are shown in Fig. 5. We can see from the plot, although among different trials, both local modes and the phonon mode are very close in energy, the variation in energy of the local modes is much larger than that of the phonon mode. The other phonon modes were checked as well, no qualitative difference was found. Thus, our observation that the V_1 mode contains a much larger Γ_0 than the other phonon modes is consistent with a mode originating from local defects.

Up to now, we have only discussed the broadening from temperature independent participation of many local modes. For the temperature dependent anharmonic coupling, it has been shown that local modes can couple to lower energy modes as has already been observed in the skutterudites,⁴¹ clathrates,⁷ and other materials.¹⁵ As the simulation shows, all the local modes are very close in energy. Therefore, one expects these modes to follow the same temperature dependence as it is driven by Bose-Einstein statistics with nearly identical energies.¹⁵ Consequently, even though the V_1 mode profile in theory consists of many modes, these modes broaden and soften with the same pace as the temperature rises. Thus, the temperature dependent behavior of the V_1 mode can still be explained by Klemens’s model.

After clarifying the origin of the anomalous line-width of the V_1 mode, we focus on the anharmonic behavior. Comparing the amplitude of ‘A’ and ‘C’ among the four modes, we find that they monotonically increase with mode energy. This is because the anharmonic coefficients are determined by the phonon joint density of states, $JD(\omega) = \sum \delta(\omega - \omega_1 - \omega_2)$. Here, ω_1 and ω_2 are the energies of the two phonons that the phonon ω decays into. $JD(\omega)$ normally is a monotonically increasing function of ω . Thus, the anharmonic coefficients are likely to be a monotonically increasing function of ω which is consistent with the fit results.

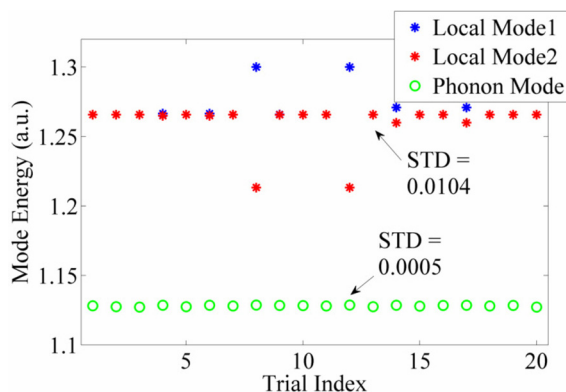


FIG. 5. Energies of local modes and a phonon mode of the one dimensional circular diatomic chain. The texts denote the corresponding standard deviation (STD).

In summary, we performed temperature dependent Raman scattering measurement on $\text{Bi}_2\text{Te}_2\text{Se}$. Four modes were observed in the entire temperature range. Three of them were assigned as the zone center modes. The extra mode (V_1) was shown most likely to be an antisite defects-induced local mode. The anomalous broadness of the local mode was clarified through a simple model of diatomic chains. The temperature dependence of the four modes was explained by an anharmonic phonon-phonon interaction model. Inelastic neutron scattering studies on $\text{Bi}_2\text{Te}_2\text{Se}$ are clearly called for to help elucidate the true nature of this mode and its role in other properties of the material such as thermal transport.

Work at the University of Toronto was supported by NSERC and CFI. The work at Princeton was supported by the NSF-sponsored MRSEC program, Grant No. DMR-1420541. K.S.B. acknowledges the support from the National Science Foundation (Grant No. DMR-1410846).

- ¹H. J. Goldsmid, *Introduction to Thermoelectricity* (Springer Science & Business Media, 2009), Vol. 121.
- ²S. Jia, H. Ji, E. Climent-Pascual, M. K. Fuccillo, M. E. Charles, J. Xiong, N. P. Ong, and R. J. Cava, *Phys. Rev. B* **84**, 235206 (2011).
- ³O. Sokolov, S. Y. Skipidarov, N. Duvankov, and G. Shabunina, *J. Cryst. Growth* **262**, 442 (2004).
- ⁴S. Nakajima, *J. Phys. Chem. Solids* **24**, 479 (1963).
- ⁵Z. Ren, A. A. Taskin, S. Sasaki, K. Segawa, and Y. Ando, *Phys. Rev. B* **82**, 241306 (2010).
- ⁶W. Richter and C. Becker, *Phys. Status Solidi B* **84**, 619 (1977).
- ⁷T. Takabatake, K. Suekuni, T. Nakayama, and E. Kaneshita, *Rev. Mod. Phys.* **86**, 669 (2014).
- ⁸W. Li and N. Mingo, *Phys. Rev. B* **89**, 184304 (2014).
- ⁹A. Hushur, M. H. Manghnani, and J. Narayan, *J. Appl. Phys.* **106**, 054317 (2009).
- ¹⁰T. Oznuluer, E. Pince, E. O. Polat, O. Balci, O. Salihoglu, and C. Kocabas, *Appl. Phys. Lett.* **98**, 183101 (2011).
- ¹¹Y. Tian, M. J. Gray, H. Ji, R. J. Cava, and K. S. Burch, “Magneto-Elastic Coupling in a ferromagnetic insulator, potential 2D Atomic Crystal,” preprint arXiv:1410.1898 (2014).
- ¹²J. Lin, L. Guo, Q. Huang, Y. Jia, K. Li, X. Lai, and X. Chen, *Phys. Rev. B* **83**, 125430 (2011).
- ¹³A. C. Ferrari and D. M. Basko, *Nat. Nanotechnol.* **8**, 235 (2013).
- ¹⁴S. Reich and C. Thomsen, *Philos. Trans. R. Soc., A* **362**, 2271 (2004).
- ¹⁵A. Barker, Jr. and A. J. Sievers, *Rev. Mod. Phys.* **47**, S1 (1975).
- ¹⁶Y. Kim, X. Chen, Z. Wang, J. Shi, I. Miotkowski, Y. P. Chen, P. A. Sharma, A. L. Lima Sharma, M. A. Hekmaty, Z. Jiang, and D. Smirnov, *Appl. Phys. Lett.* **100**, 071907 (2012).
- ¹⁷A. A. Reijnders, Y. Tian, L. J. Sandilands, G. Pohl, I. D. Kivlichan, S. Y. F. Zhao, S. Jia, M. E. Charles, R. J. Cava, N. Alidoust, S. Xu, M. Neupane, M. Z. Hasan, X. Wang, S. W. Cheong, and K. S. Burch, *Phys. Rev. B* **89**, 075138 (2014).
- ¹⁸P. Zareapour, A. Hayat, S. Y. F. Zhao, M. Kreshchuk, Y. K. Lee, A. A. Reijnders, A. Jain, Z. Xu, T. Liu, G. Gu *et al.*, *Phys. Rev. B* **90**, 241106 (2014).
- ¹⁹L. Sandilands, J. Shen, G. Chugunov, S. Zhao, S. Ono, Y. Ando, and K. Burch, *Phys. Rev. B* **82**, 064503 (2010).
- ²⁰C. Beekman, A. Reijnders, Y. Oh, S. Cheong, and K. Burch, *Phys. Rev. B* **86**, 020403 (2012).
- ²¹L. J. Sandilands, Y. Tian, K. W. Plumb, Y.-J. Kim, and K. S. Burch, *Phys. Rev. Lett.* **114**, 147201 (2015).
- ²²Y. Tian, A. A. Reijnders, M. E. Holmes, I. Valmianski, J. G. Ramirez, C. Urban, R. Zhong, J. Schneeloch, G. Gu, I. K. Schuller, I. Henslee, and K. S. Burch, “Ultra-stable high NA automated variable temperature Raman microscope” (unpublished).
- ²³V. Gnezdilov, Y. G. Pashkevich, H. Berger, E. Pomjakushina, K. Conder, and P. Lemmens, *Phys. Rev. B* **84**, 195118 (2011).
- ²⁴O. Hellman and D. A. Broido, *Phys. Rev. B* **90**, 134309 (2014).
- ²⁵H. Shi, D. Parker, M.-H. Du, and D. J. Singh, *Phys. Rev. Appl.* **3**, 014004 (2015).

- ²⁶A. Akrap, M. Tran, A. Ubaldini, J. Teyssier, E. Giannini, D. Van Der Marel, P. Lerch, and C. C. Homes, *Phys. Rev. B* **86**, 235207 (2012).
- ²⁷S. Zhao, C. Beekman, L. Sandilands, J. Bashucky, D. Kwok, N. Lee, A. LaForge, S. Cheong, and K. Burch, *Appl. Phys. Lett.* **98**, 141911 (2011).
- ²⁸E. M. Ferreira, M. V. Moutinho, F. Stavale, M. Lucchese, R. B. Capaz, C. Achete, and A. Jorio, *Phys. Rev. B* **82**, 125429 (2010).
- ²⁹S. Jia, H. Beidenkopf, I. Drozdov, M. Fuccillo, J. Seo, J. Xiong, N. Ong, A. Yazdani, and R. Cava, *Phys. Rev. B* **86**, 165119 (2012).
- ³⁰Y. Tian, S. Jia, R. Zhong, J. Schneeloch, G. Gu, R. J. Cava, and K. S. Burch, "Temperature dependent Raman study of Bi₂Se₃, Bi₂Te₃ and Bi₂Te₂Se" (unpublished).
- ³¹D. Feldman, M. Ashkin, and J. H. Parker, Jr., *Phys. Rev. Lett.* **17**, 1209 (1966).
- ³²H. W. Verleur and A. S. Barker, *Phys. Rev.* **155**, 750 (1967).
- ³³H. W. Verleur and A. S. Barker, *Phys. Rev.* **164**, 1169 (1967).
- ³⁴H. Trodahl, D. Pooke, G. Gainsford, and K. Kishio, *Physica C* **213**, 427 (1993).
- ³⁵H. Siegle, I. Loa, P. Thurian, G. Kaczmarczyk, L. Filippidis, A. Hoffmann, C. Thomsen, D. Schikora, M. Hankeln, and K. Lischka, *Z. Phys. Chem.* **200**, 187 (1997).
- ³⁶C. Sudakar, P. Kharel, G. Lawes, R. Suryanarayanan, R. Naik, and V. Naik, *J. Phys.: Condens. Matter* **19**, 026212 (2007).
- ³⁷M. Balkanski, R. F. Wallis, and E. Haro, *Phys. Rev. B* **28**, 1928 (1983).
- ³⁸S. Usher and G. P. Srivastava, *Phys. Rev. B* **50**, 14179 (1994).
- ³⁹P. G. Klemens, *Phys. Rev.* **148**, 845 (1966).
- ⁴⁰S.-I. Tamura, *Phys. Rev. B* **27**, 858 (1983).
- ⁴¹N. Ogita, R. Kojima, T. Hasegawa, Y. Takasu, M. Udagawa, T. Kondo, S. Narazu, T. Takabatake, N. Takeda, Y. Ishikawa *et al.*, *J. Phys. Soc. Jpn.* **77**, 251 (2008).